J. Fluid Mech. (1980), *vol.* 99, *part* 4, *pp.* 817–840
Printed in Great Britain

Autorotation of an elliptic cylinder about an axis perpendicular to the flow

By HANS J. LUGT

David W. Taylor Naval Ship Research and Development Center,
Bethesda, Maryland 20084, U.S.A.

(Received 17 May 1979 and in revised form 9 November 1979)

Autorotation of an elliptic cylinder about an axis fixed perpendicular to a parallel flow is explained in this paper by means of numerical solutions of the Navier–Stokes equations. Potential-flow theory predicts, for constant angular velocity, half a period in which a torque supports rotation and half a period in which it opposes rotation, with vanishing torque in the average. This balance is disturbed by viscous-flow effects in such a way that, for a given angular velocity, vortex shedding either damps rotation or, under certain conditions, favours rotation. The proper interplay of those conditions, which include synchronization of vortex shedding and rate of rotation, results in autorotation. The numerical results for $Re \leqslant 400$ are compared with experimental data for $Re = 90000$ from the literature. The agreement of the force coefficients and the large-scale flow patterns is surprisingly good.

1. Background

The concept of autorotation is not uniquely defined in fluid dynamics. Sometimes, aerodynamicists consider any continuous rotation of a body in a parallel flow without external sources of energy as autorotation. Under this definition, windmills, water wheels, anemometers, and certain tree fruits and seeds are 'autorotating' devices. These bodies are geometrically shaped in such a way that, whenever they are kept fixed in a fluid flow, a torque is present which initiates rotation as soon as the bodies are released. On the other hand, a body can exhibit autorotation in the classical sense only if one or more stable positions exist at which the fluid flow exerts no torque on the resting body. In this case, a sufficiently strong initial impulse is required before the fluid flow can maintain a continuous spinning of the body.

Although the axis of rotation may assume any orientation with respect to the flow, it is useful to distinguish two special cases of axis orientation for autorotation in the restricted, classical sense. In the first special case the axis of rotation is parallel to the flow, and the body must be symmetrical with regard to the parallel stream such that no torque is present whenever the body is at rest. An initial impulse is always necessary to obtain autorotation. Typical examples are the Lanchester propeller (Riabouchinsky 1935) and the spinning airfoil (Bairstow 1939). The explanation of these phenomena is quite straightforward; it is based on the local change of angle of attack of the rotating wing and on the occurrence of stall.

In the second special case the axis is perpendicular to the parallel flow and the body need be symmetrical with respect to the parallel flow in only one stable position. In this position the flow exerts no torque on the resting body, and again an initial impulse

0022-1120/80/4516-1770 $02.00

is necessary to obtain autorotation. However, from other positions, the body will start rotating when released with no initial impulse, provided the body can pick up and store sufficient angular momentum to overcome the adverse torque around the stable position. Examples are the falling rectangular piece of cardboard and the rotating dumb-bell (A. M. O. Smith 1953). The axis of the cardboard (or plate) may be free to move or may be fixed in a parallel stream. The autorotation of the dumb-bell is due to the sudden drop of the spheres' drag in the transition range from laminar to turbulent flow and, thus, is restricted to the Reynolds-number region of about 4×10^5. The explanation of the plate autorotating around an axis fixed in the stream is given in this paper.

A few historical notes on the autorotation of plates will inform the reader of the physical problems involved and of the areas of application. A detailed historical account has been given by Lugt (1978).

Maxwell (1890) was probably the first to describe a falling rotating rectangular piece of cardboard in 1853. He recognized that the centre of mass and the centre of aerodynamic forces do not coincide. This gives rise to a torque. He assumed that this torque can be divided into a 'quasi-steady' part and a contribution due to rotation which is called the 'dynamic' part. The latter is, according to Maxwell, always opposite to the direction of rotation. 'Quasi-steady' means that the forces on the body vary so slowly with rotation that they can be computed at a particular instant as if the body were not rotating. From angles of attack $\alpha = 0°$ to $90°$ the torque on the plate supports rotation ('supporting period'), whereas from $\alpha = 90°$ to $180°$ the torque acts on the plate in opposition to rotation ('retarding period'). Maxwell argued that the torque in the supporting period is larger than in the retarding period because the translational velocity of the plate for $\alpha = 0°$ is larger (the drag is smaller) than that for $\alpha = 90°$. The higher translational speed around $\alpha = 0°$ causes a larger torque in the supporting period. Maxwell also recognized that the deviation from vertical fall is attributable to the lift due to rotation.

Riabouchinsky (1935), who about 1906 coined the word 'autorotation', distinguished for the first time between autorotating plates with fixed axes and those with freely moving axes. He realized that Maxwell's explanation was deficient in that, for autorotation with fixed axes, there is no net supporting torque for the quasi-steady part. The dynamic part, however, gives a supporting contribution since, in the supporting period from $\alpha = 0°$ to $90°$, the streamlines at the leading edge of the plate are more curved than those at the same α in the retarding period. Hence, the larger suction effect at the leading edge causes a higher torque in the supporting period. Although Riabouchinsky's statement is true, i.e. the dynamic part can contribute to a net supporting torque, the explanation for it is too vague. He also found that the moment of inertia must be large enough to overcome the period of adverse torque (fly-wheel effect).

After World War II considerable interest in autorotation normal to a parallel flow arose in three different technical areas. The largest effort was devoted to the control of spinning finned missiles, followed by investigations of the spreading of autorotating leaflets, bomblets, and seeds. The third area dealt with the autorotating behaviour of non-stabilized airships, re-entry bodies, released nose sections of fuselages, and hail-stones of oblate-spheroidal shape. A compilation of the extensive literature can be found in the report by Lugt (1978). From this literature, a few results of importance to the explanation of autorotating plates are summarized here.

A. M. O. Smith (1953) recognized that lift hysteresis is an essential effect in understanding autorotation. In the late fifties, ciné films (unpublished) of wind-tunnel experiments with plates and cruciform plate systems were made at the Department of Aeronautical Engineering at the University of Notre Dame, Indiana, under the direction of F. N. M. Brown. These movies clearly reveal the existence and attachment of a strong vortex at the receding edge of the plate in the retarding period. Detailed experimental studies with autorotating plates were made by E. H. Smith (1971) which produced data on drag, lift, and moment coefficients as a function of angle of attack. The influence of Reynolds number, moment of inertia, and other parameters on autorotation was also investigated. During the review of this paper the investigation by Iversen (1979) came to the attention of the author. Iversen analysed experimental data from previous studies and evaluated them with respect to effects of Reynolds number, moment of inertia, and geometry on autorotation.

The state-of-the-art today may be summarized in the following way. Autorotation about an axis perpendicular to the fluid flow can be explained qualitatively for bodies with freely moving axes by means of the 'quasi-steady' method if the dimensionless moment of inertia is small (but not so small that the body will oscillate instead of autorotate). For large values of moment of inertia the freely moving body behaves like one with a fixed axis, and the quasi-steady theory is not valid. Some aspects of the dynamic behaviour are fairly well understood, for instance the role of lift hysteresis. However, a detailed and complete explanation is still lacking. The present paper will address this deficiency.

It is interesting to note that this study is an example of the way in which computer experiments can help to explain phenomena which are too difficult or too costly to study by means of physical experiments.

2. Model formulation and solution technique

The movement of a freely falling rectangular piece of cardboard indicates that the autorotation around the spanwise axis is quite stable, and that the model can be simplified by assuming the laminar flow of an incompressible fluid around an infinitely long plate in two space dimensions. Since autorotation of a plate about a fixed axis cannot be explained by a quasi-steady theory, the assumption of a fixed axis focuses the study on the essential features which generate autorotation. Under this assumption the motion of the body has one degree of freedom, that is, the body rotates only about the fixed axis with the angular velocity $\Omega = d\alpha/dt'$, where α is the angle of attack and t' the time. The equation for the angular motion is then

$$I\,d\Omega/dt' = T, \tag{1}$$

where I is the moment of inertia and T the torque. For periodic motions of the plate autorotation is defined by

$$\bar{T} = \frac{1}{2\pi}\int_0^{2\pi} T\,d\alpha = 0. \tag{2}$$

In general, of course, the value of the integral $\int_0^{\alpha} T\,d\tilde{\alpha}$ is not zero except for certain values of α. Riabouchinsky (1935) noticed that I must be sufficiently large if the plate

is to autorotate. The experiments of E. H. Smith (1971) show, furthermore, that Ω is almost constant under certain conditions. Criteria for autorotation and $\Omega \approx$ const. can be obtained from equation (1) by integration with respect to α:

$$\Omega^2 = \bar{\Omega}^2 + \frac{2}{I}\int_{\alpha_M}^{\alpha} T\, d\tilde{\alpha}. \tag{3}$$

Here α_M is the angle of attack at which Ω is equal to the average value $\bar{\Omega}$. (Equation (3) was given by A. M. O. Smith (1953) for $\alpha_M = 0°$, $\Omega = \Omega_0$.) Introducing the moment coefficient $C_M = T/\frac{1}{2}\rho U^2(\frac{1}{2}d)^2$, the spin parameter $S = \bar{\Omega}d/2U$, and the dimensionless moment of inertia $I^* = I/\rho(\frac{1}{2}d)^4$, one obtains for equation (3):

$$\left(\frac{\Omega}{\bar{\Omega}}\right)^2 = 1 + \frac{1}{I^*S^2}\int_{\alpha_M}^{\alpha} C_M\, d\tilde{\alpha}, \tag{4}$$

with ρ the density of the fluid, U the constant speed of the parallel flow, and d the chord of the plate. Since the integral in equation (4) is a periodic function with finite amplitude $B > 0$, it follows from equation (4) that

$$\left(1 - \frac{B}{I^*S^2}\right)^{\frac{1}{2}} \leqslant \frac{\Omega}{\bar{\Omega}} \leqslant \left(1 + \frac{B}{I^*S^2}\right)^{\frac{1}{2}}. \tag{5}$$

Autorotation differs from oscillation in that with autorotation Ω never changes its sign. Hence, if one assumes without loss of generality that $\Omega > 0$, the condition for autorotation is

$$\frac{B}{I^*S^2} \leqslant 1. \tag{6}$$

The stronger restriction that $\Omega \approx \bar{\Omega}$ is

$$\frac{B}{2I^*S^2} \ll 1, \tag{7}$$

which usually requires a large moment of inertia, that is, $I^* \gg 1$. E. H. Smith's experiments show that the fluctuation of Ω is about 2 % of $\bar{\Omega}$ for the special arrangement he used. An evaluation of his data also reveals that B is almost constant over a wide Reynolds-number range, and that the Reynolds number can be as low as

$$Re_d = Ud/\nu = 100,$$

where ν is the kinematic viscosity of the fluid.

The occurrence of autorotation at low Reynolds numbers permits the construction of solutions of the Navier–Stokes equations with presently available computers and experience in numerical analysis. The assumption of constant Ω overcomes another difficulty in numerical formulations and solutions: In order to induce the plate to autorotate a certain amount of initial rotation must be provided. If this initial impulse is too weak, the plate will oscillate a few times, and the motion may then come either to a stop or it may become autorotation. If the initial rotation is too strong, the plate will first rotate owing to this initial impulse and may subsequently autorotate. In both cases numerical computations would require a number of trials with excessively long computer runs to arrive at a solution for the state of autorotation. This situation can be avoided by assuming a constant Ω of the plate. Then, only the Reynolds number,

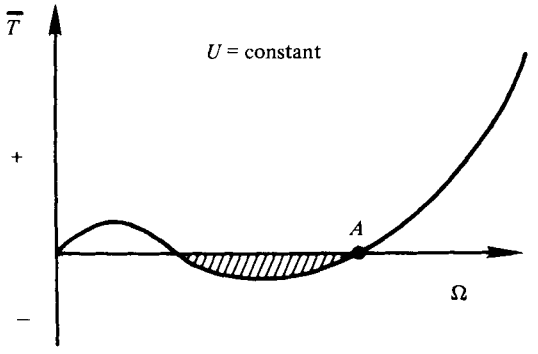

FIGURE 1. Average torque $\bar{T}$ plotted versus Ω. A positive value of $\bar{T}$ means that an outside torque is necessary to drive the plate with constant angular velocity Ω. Negative values of $\bar{T}$ (shaded area) indicate that the outside torque has a breaking effect. If in this area the body is free to rotate, it will autorotate and increase its angular velocity until point A is reached. This is the stable state of autorotation (after Riabouchinsky 1935).

the spin parameter, and the geometric quantities occur as flow parameters after the initial phase.†

In general, equation (2) will not be satisfied for a prescribed set of flow parameters if Ω is a constant. Rather, $\bar{T}$ can be positive, in which case the plate must be driven by an external force, or $\bar{T}$ can be negative, in which case the external force will cause braking. Riabouchinsky (1935) experimented with the Lanchester propeller and obtained a relation between $\bar{T}$ and Ω as sketched in figure 1. When Ω is small or large in relation to U, an outside positive torque is necessary to drive the plate. Between these values, an Ω range exists in which the outside torque is negative and thus requires a braking effect on the spinning of the propeller. Riabouchinsky called this range 'autorotative'. If the outside torque were removed, the propeller would increase its angular velocity until $\bar{T} = 0$, which is the state of autorotation (point A in figure 1). Since a second situation exists in which $\bar{T} = 0$, the condition of autorotation must be augmented by the stability criterion $(\partial \bar{T}/\partial \Omega)_{\bar{T}=0} > 0$.

The same situation, observed by Riabouchinsky for the Lanchester propeller, holds also for the plate rotating about a fixed axis normal to the flow. Thus, the phenomenon of autorotation can be studied by examining the flow behaviour for various values of S.

For numerical reasons, as given by Lugt & Ohring (1977), it is convenient to approximate the plate by a thin elliptic cylinder in a co-ordinate system (η, θ) which is related to the Cartesian co-ordinates (x, y) through

$$x + iy = a \cosh(\eta + i\theta) \quad \text{for} \quad a > 0, \tag{8}$$

where a is the focal distance; $\eta = \eta_1$ is the elliptic body contour. Its value is also a measure of the relative thickness of the 'plate'. Again for numerical reasons, $\eta_1 = 0{\cdot}1$ was chosen (except for one case with $\eta_1 = 0{\cdot}6$) instead of $\eta_1 = 0$, which is the infinitely thin plate. However, it may be mentioned that the difference in the results between $\eta_1 = 0$ and $\eta_1 = 0{\cdot}1$ is insignificant.

† It should be pointed out, however, that with Ω = const. the effect of changes in the moment of inertia cannot be obtained.

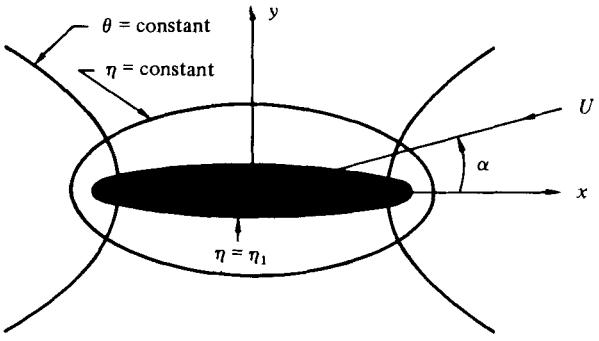

FIGURE 2. Elliptic co-ordinate system and definition of angle of attack α. In this figure the right-hand edge of the elliptic cylinder is the 'leading edge' for $0° \leqslant \alpha < 90°$ and $270° < \alpha \leqslant 360°$, and becomes the 'trailing edge' for $90° < \alpha < 270°$. The upper half of the surface which faces the flow is called the 'front', the lower half the 'rear' of the body. A vortex which develops in the rear of an edge develops 'behind' this edge. The edge which moves with the flow is called the 'retreating edge' (the right-hand edge in the figure), the other edge is the 'advancing edge'.

If the reference frame is fixed to the body, the initial- and boundary-value problem for the Navier–Stokes equations expressed in terms of the vorticity ω and the stream function ψ is

$$\frac{\partial \omega}{\partial t} + \frac{1}{h^2}\frac{\partial(\psi, \omega)}{\partial(\eta, \theta)} = \frac{2}{Re}\nabla^2\omega, \tag{9}$$

$$\nabla^2\psi = \omega, \tag{10}$$

where the flow quantities are made dimensionless by U and the focal distance a. In particular, $t = t'U/a$. The Reynolds number is defined by $Re = 2aU/\nu$, and the parameter h is $h^2 = \cosh^2\eta - \cos^2\theta$.

The spin parameter S enters into the boundary conditions. In Lugt & Ohring (1977) the Rossby number $Ro = U/a\Omega$ was introduced. However, for practical reasons, it is useful to have the chord of the plate $d = 2a\cosh\eta_1$ as a reference length. Then, $Re_d = dU/\nu$, $S = 1/Ro_{\frac{1}{2}d} = d\Omega/2U$. The boundary conditions are (figure 2):

$$\psi = 0, \quad \partial\psi/\partial\eta = 0 \quad \text{at} \quad \eta = \eta_1, \tag{11}$$

$$\left.\begin{aligned} h^{-1}\,\partial\psi/\partial\theta &= \cos(\theta - t/Ro), \\ h^{-1}\,\partial\psi/\partial\eta &= \sin(\theta - t/Ro) + (h\,Ro)^{-1}\cosh\eta\sinh\eta \end{aligned}\right\} \quad \text{at} \quad \eta = \infty \tag{12}$$

with $\alpha(t) \equiv t/Ro$ the angle of attack.

The abrupt start of the body from rest is chosen as the initial condition, which consists of the potential-flow solution and a vorticity sheet at the body surface enforcing the nonslip condition. Part of the initial condition is the initial angle of attack $\alpha = \alpha_0$. In all examples α_0 is chosen to be 0°, since for this angle the transient period is short compared with that for $\alpha = \frac{1}{2}\pi$ (Lugt & Ohring 1977).

The drag, lift and moment coefficients are defined by

$$\left.\begin{aligned} C_D &= -\text{drag}/\tfrac{1}{2}\rho U^2(\tfrac{1}{2}d), \\ C_L &= -\text{lift}/\tfrac{1}{2}\rho U^2(\tfrac{1}{2}d), \\ C_M &= \text{torque}/\tfrac{1}{2}\rho U^2(\tfrac{1}{2}d)^2. \end{aligned}\right\} \tag{13}$$

Each of the coefficients in equation (13) consists of two parts. The drag coefficient is the sum of the drag due to pressure and the drag due to friction

$$C_D = C_{DP} + C_{DF} \tag{14}$$

with

$$C_{DP} = -2\tanh\eta_1 \cos\alpha \int_0^{2\pi} p_1 \cos\theta\, d\theta - 2\sin\alpha \int_0^{2\pi} p_1 \sin\theta\, d\theta,$$

$$= \frac{4}{Re}\left[\tanh\eta_1 \cos\alpha \int_0^{2\pi} \left(\frac{\partial\omega}{\partial\eta}\right)_1 \sin\theta\, d\theta - \sin\alpha \int_0^{2\pi} \left(\frac{\partial\omega}{\partial\eta}\right)_1 \cos\theta\, d\theta\right], \tag{15}$$

$$C_{DF} = \frac{4}{Re}\left[-\cos\alpha \int_0^{2\pi} \omega_1 \sin\theta\, d\theta + \tanh\eta_1 \sin\alpha \int_0^{2\pi} \omega_1 \cos\theta\, d\theta\right]. \tag{16}$$

The lift and moment coefficients may be expressed in a corresponding way (Lugt & Haussling 1974). In this notation, positive values of C_D, C_L, and C_M denote, respectively, drag, lift in the direction of the Magnus force, and torque counteracting the body rotation.

The initial- and boundary-value problem defined above is solved by the same finite-difference scheme used in an earlier paper (Lugt & Ohring 1977). It is, therefore, not necessary to repeat the procedure here, but it may be mentioned that the vorticity equation (9) is discretized with the Dufort–Frankel scheme, and that the Poisson equation (10) is solved with Hockney's direct method. Furthermore, the following transformation is made for numerical reasons:

$$\psi = \psi^* + 2/Ro\,(\cosh^2\eta - \sin^2\theta), \tag{17}$$

$$\omega = \omega^* + 2/Ro. \tag{18}$$

This transformation avoids large values of ψ at the outer boundary but leaves the grid fixed to the body.

The grid has been chosen in such a way that the infinite region of integration is replaced by a finite network of points $\eta_1 + (i-1)\,\Delta\eta$, $(j-\frac{1}{2})\,\Delta\theta$ with $i = 1, \ldots, 97$ and $j = 1, \ldots, 96$; $\Delta\eta = 0{\cdot}04$. The time increments, except in the brief initial phase where they are very small, are:

$S = 1, 0{\cdot}5, 0{\cdot}25,$	$\eta_1 = 0{\cdot}1,$	$\Delta t = 0{\cdot}0025;$
$S = 0{\cdot}167,$		$\Delta t = 0{\cdot}003;$
$S = 0{\cdot}5,$	$\eta_1 = 0{\cdot}6,$	$\Delta t = 0{\cdot}005.$

Since $\Delta\alpha = \Delta t/Ro$, more computer time is required to calculate one plate revolution at higher Rossby number. The computer time required on the IBM 360-91 for each time step is 0·7 s. One cycle, equal to half a plate revolution, requires then 1250 time-steps times $0{\cdot}7 \times Ro$, which is $870 \times Ro$ s.

The accuracy of the numerical scheme was previously checked for the non-rotating plate by comparing results using varying grids, with experimental results by Honji (Lugt & Haussling 1974), and with a different numerical scheme by Mehta of Stanford University (private communication) and by Collins & Dennis (Lugt & Haussling 1978). The general rotating-plate program was checked for the special case of the rotating circular cylinder (Lugt & Ohring 1977).

Ro	S	Re	Re_d	η_1	Range
1	~ 1	200	~ 200	0·1	$0°$–$5{\cdot}5\pi$
2	$\sim 0{\cdot}5$	400	~ 400	0·1	$0°$–4π
4	$\sim 0{\cdot}25$	200	~ 200	0·1	$0°$–$2{\cdot}2\pi$
6	$\sim 0{\cdot}167$	200	~ 200	0·1	$0°$–$1{\cdot}5\pi$
2·37	0·5	169	200	0·6	$0°$–6π

TABLE 1

The following cases, in addition to those published in Lugt & Ohring (1977), have been computed, see table 1. The results are presented in the form of flow patterns for streamlines and equi-vorticity lines with ψ^* values of $-3{\cdot}0, -2{\cdot}8, \ldots, 0, \ldots, 2{\cdot}8, 3{\cdot}0$ and with ω^* values of $-11{\cdot}0, -9{\cdot}0, \ldots, 9{\cdot}0, 11{\cdot}0$. In addition, the moment coefficients and some data on the surface pressure are given.

Since there exists no preferred reference frame in which to present the streamlines, the selection of such a frame depends on how useful it is for discussions of the flow patterns. Two different reference frames have been chosen: (1) a frame fixed to the centre of the body, but rotating in relation to the plate; and (2) a frame fixed to the body.

3. Results

In figure 3 the moment coefficients C_M for $S = 1, 0{\cdot}5, 0{\cdot}25, 0{\cdot}167$ are plotted against the angle of attack α for several revolutions. The transient phase after the abrupt start is short, approximately $t = \alpha\, Ro = \pi$ with $t_0 = 0$, $\alpha_0 = 0°$. Hence for the largest Ro computed, that is $Ro = 6$, the initial phase extends only from $\alpha = 0°$ to $30°$, and the computation of one cycle afterwards is sufficient. However, variations in the amplitude, which can occur after the initial phase, are probably due to the development of the wake and should vanish after a certain time.

In figure 4 a representative cycle of C_M (half revolution) is plotted for $S = 1, 0{\cdot}5, 0{\cdot}25, 0{\cdot}167$, $Re = 200$, $\eta_1 = 0{\cdot}1$. These values are much smaller than those predicted by the potential-flow solution

$$C_M = -\pi \sin 2\alpha \tag{19}$$

for a thin plate either fixed or rotating with constant Ω. This torque is generated through the asymmetric locations of the stagnation points which are not affected by the rotation term in the stream function because of its symmetry (Lamb 1945). The amplitude of the function (19) is $C_M \approx -\pi$ for $\eta_1 = 0{\cdot}1$. In figure 4 values for a non-rotating body at $\alpha = 45°$ and $135°$ are also included. These values vary according to the periodic wake of the vortex street.

The average value of C_M is defined by

$$\bar{C}_M = \frac{1}{2\pi} \int_{2\pi n}^{2\pi(n+1)} C_M \, d\alpha, \quad n = 0, 1, \ldots . \tag{20}$$

It is zero for the potential-flow solution (19) which characterizes autorotation. For viscous fluid flows the average values of C_M are presented in figure 5 as a function of

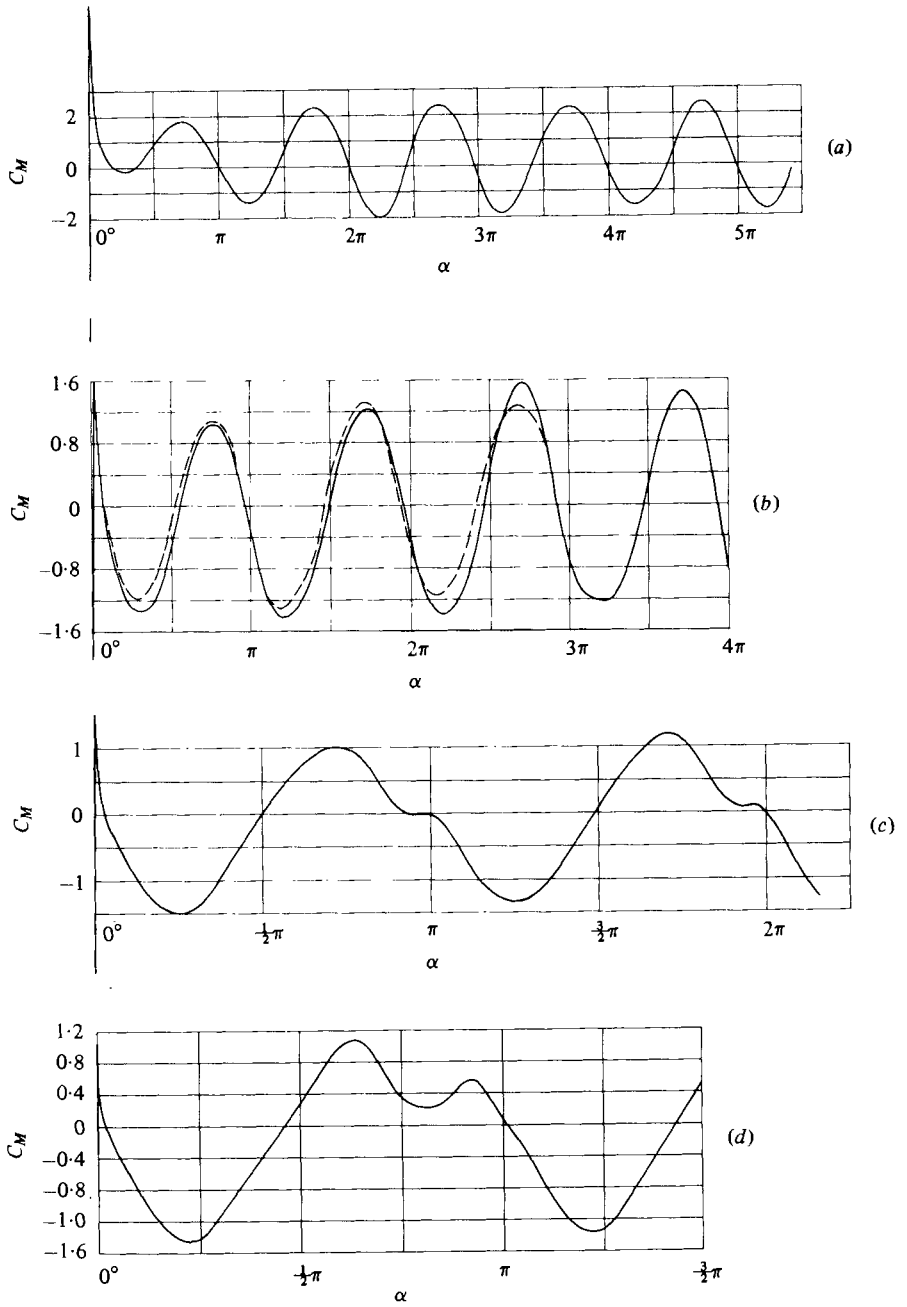

FIGURE 3. C_M *versus* α for $\eta_1 = 0{\cdot}1$, $\alpha_0 = 0°$. (*a*) $S = 1$, $Re = 200$. (*b*) $S = 0{\cdot}5$: ——, $Re = 400$; – – –, $Re = 200$. (*c*) $S = 0{\cdot}25$, $Re = 200$. (*d*) $S = 0{\cdot}167$, $Re = 200$.

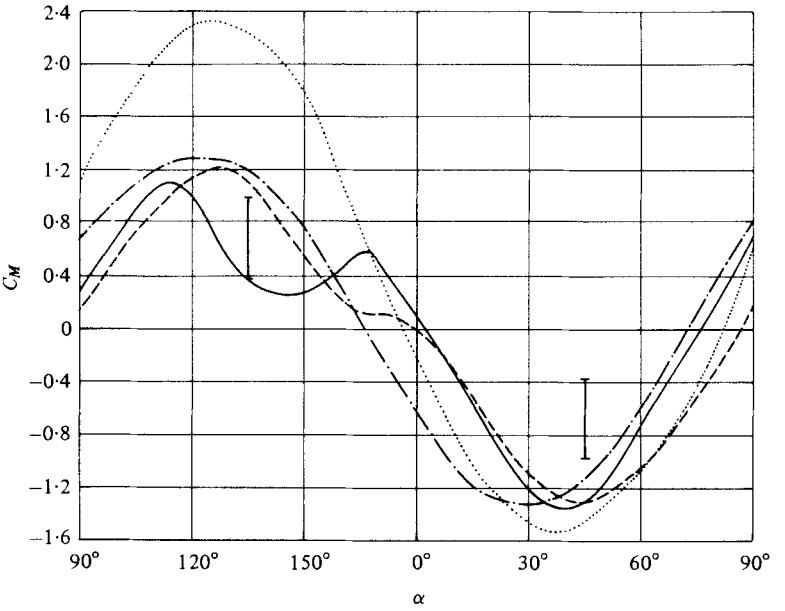

FIGURE 4. Comparison of C_M *versus* α over one representative cycle (half revolution of the plate) for various S with $Re = 200$, $\eta_1 = 0{\cdot}1$. The retarding period extends approximately from 90° to 180° (0°), the supporting period from 0° to 90°. · · · · ·, $S = 1$; —·—·—, $S = 0{\cdot}5$; – – –, $S = 0{\cdot}25$; ——, $S = 0{\cdot}167$; I, fixed plate.

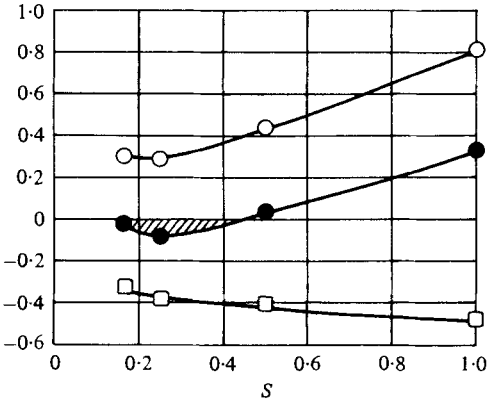

FIGURE 5. Moment coefficients *versus* S for $Re = 200$, $\eta_1 = 0{\cdot}1$. ○, $\bar{C}_{MR}$; □, $\bar{C}_{MS}$; ●, $\bar{C}_M$. In the shaded area the body autorotates. (See also the legend for figure 1.)

S for $Re = 200$. It is useful to distinguish between the retarding and supporting periods of C_M:

$$\bar{C}_{MR} = \frac{1}{2\pi}\int_{2\pi n}^{2\pi(n+1)} \begin{cases} C_M & \text{for } C_M > 0 \\ 0 & \text{for } C_M \leqslant 0 \end{cases} d\alpha,$$

$$\bar{C}_{MS} = \frac{1}{2\pi}\int_{2\pi n}^{2\pi(n+1)} \begin{cases} C_M & \text{for } C_M \leqslant 0 \\ 0 & \text{for } C_M > 0 \end{cases} d\alpha. \tag{21}$$

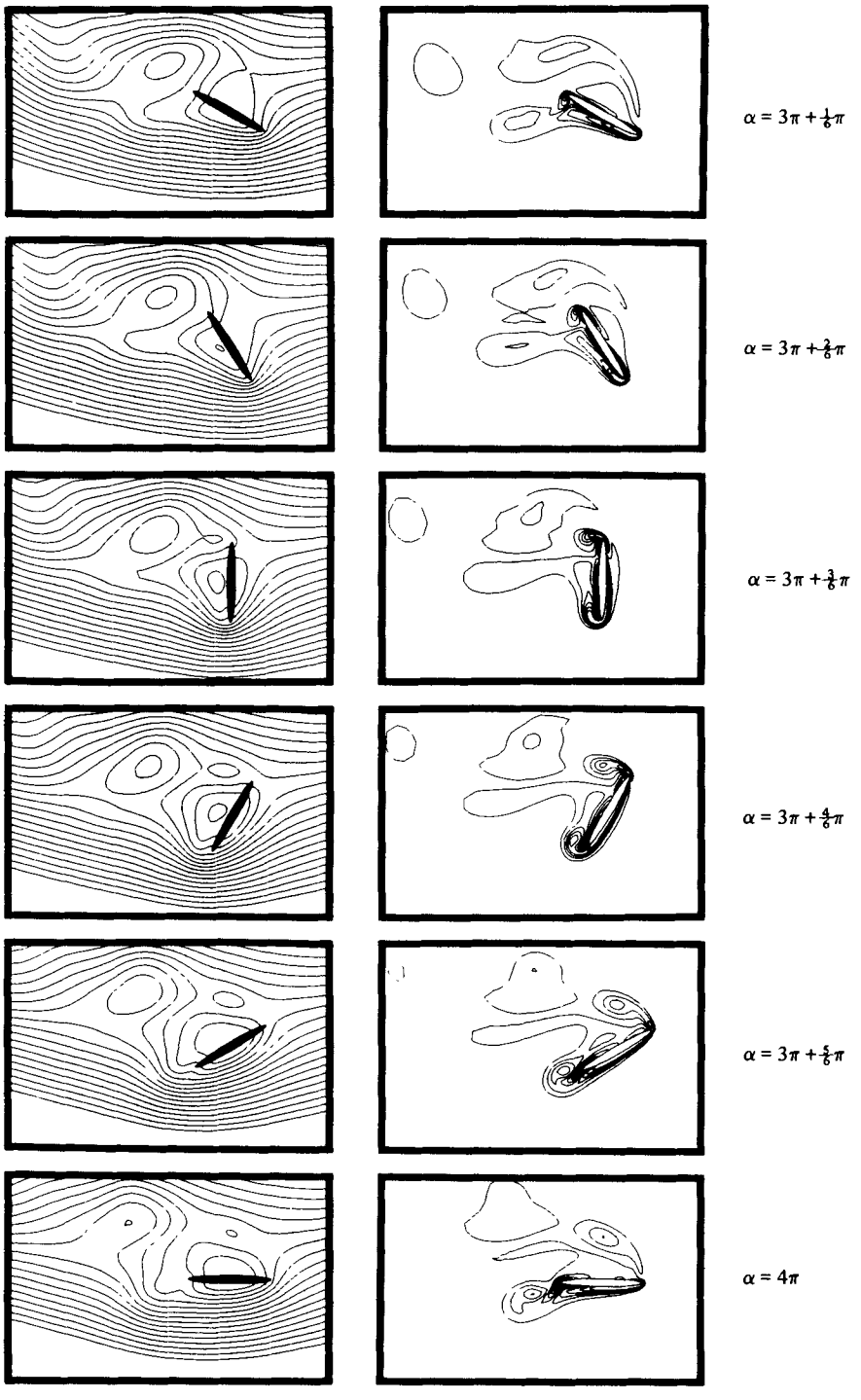

FIGURE 6. Sequence of streamlines and equi-vorticity lines around a rotating thin elliptic cylinder in a parallel flow for $S = 1$, $Re = 200$, $\eta_1 = 0{\cdot}1$, $\alpha_0 = 0°$. The flow is from right to left. In the supporting period from $\alpha = 3\pi$ to $3\pi + \frac{3}{6}\pi$ the retreating edge (lower right) is the leading edge and becomes the trailing edge (lower left) in the retarding period $3\pi + \frac{3}{6}\pi < \alpha < 4\pi$. The streamlines are computed in a frame which is fixed to the body with regard to translation but which is fixed in space with regard to rotation.

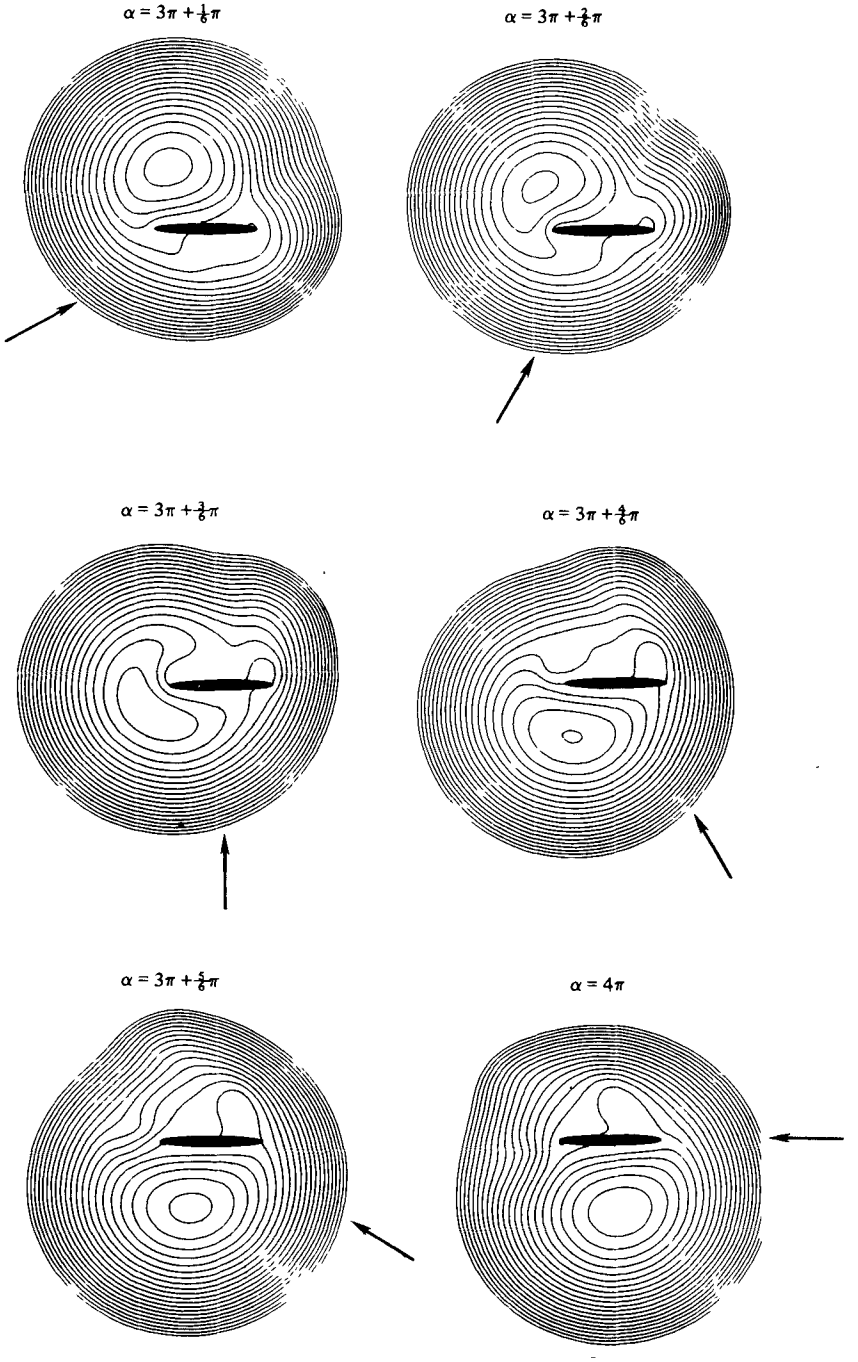

FIGURE 7. The same situation as in figure 6 but the streamlines are computed in a frame fixed to the body.

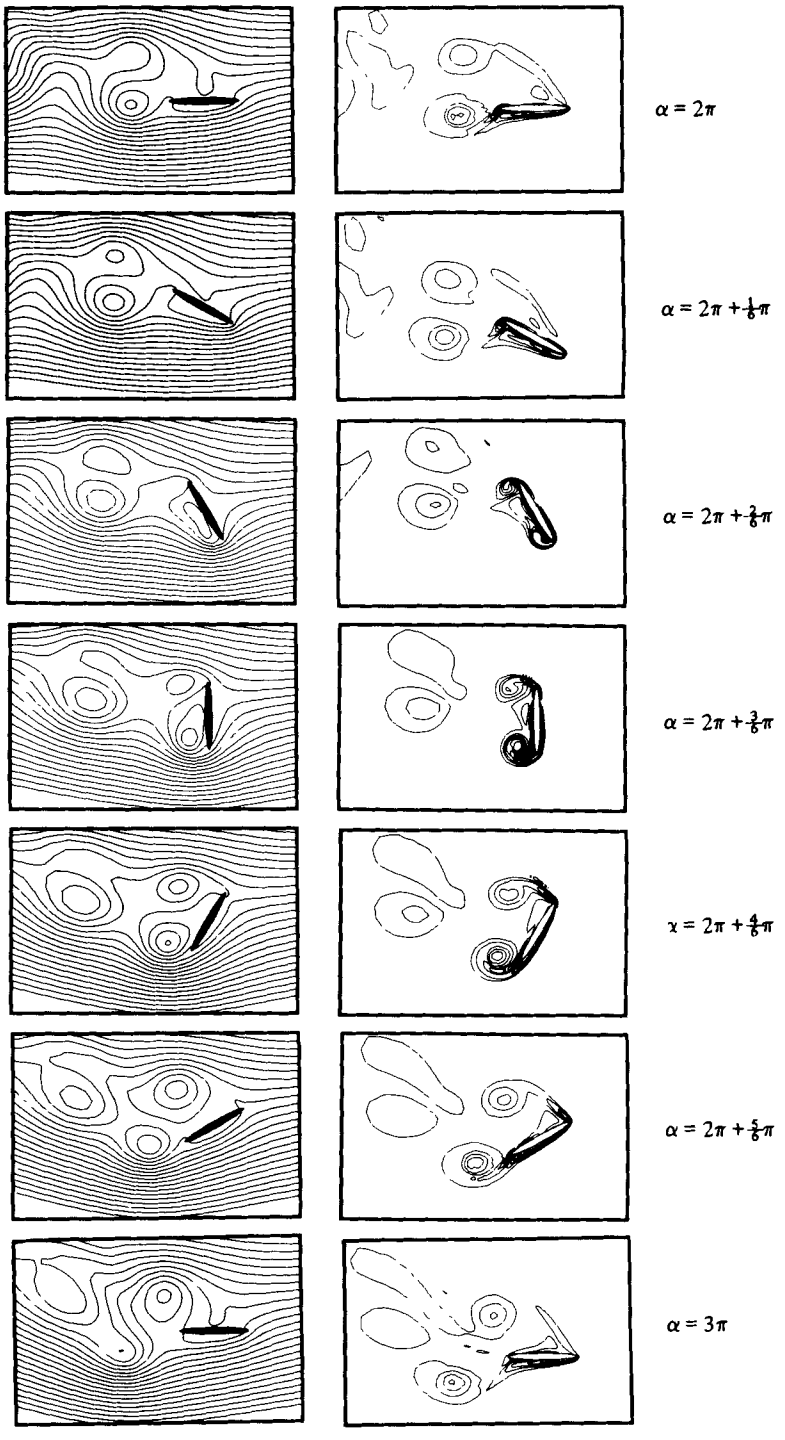

FIGURE 8. Sequence of streamlines and equi-vorticity lines for $S = 0{\cdot}5$, $Re = 400$, $\eta_1 = 0{\cdot}1$, $\alpha_0 = 0°$. The case $Re = 200$ is published in Lugt & Ohring (1977).

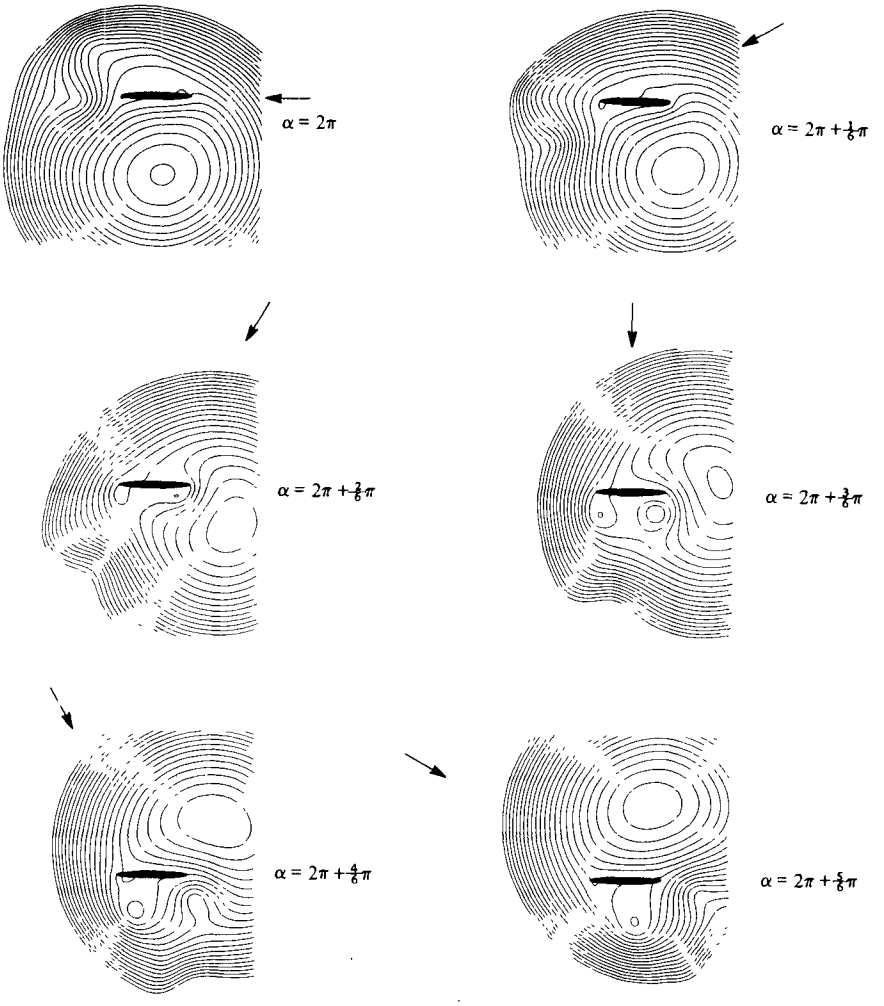

FIGURE 9. Same situation as in figure 8 but streamlines are computed in a frame fixed to the body.

Negative values of $\bar{C}_M$ appear in the shaded region with a minimum at $S = 0{\cdot}25$. Stable autorotation occurs at $S = 0{\cdot}45$. Although $\bar{C}_M$ is still negative for $S = 0{\cdot}167$, the fact that its absolute value is smaller than for $S = 0{\cdot}25$ indicates the trend toward positive values.

It may be noted that the values of the frictional parts C_{DF}, C_{LF}, and C_{MF} of the total forces and torque are an order-of-magnitude smaller than C_D, C_L, and C_M, even for the thick body $\mu_1 = 0{\cdot}6$. The following discussions are, therefore, based mainly on the pressure and the coefficient C_{MP}.

In comparing the frequency of vortex shedding with the rate of rotation, it is useful to consult the patterns of streamlines and equi-vorticity lines over a cycle for various S (figures 6–13). As already pointed out in Lugt & Ohring (1977) two types of vortex shedding can be distinguished, depending on whether the vortex at the retreating edge is in front of or behind the edge as seen from the direction of parallel flow (figure 6, $\alpha = 3\pi + \frac{5}{6}\pi$, the vorticity tongue at the lower edge curled in the counter-clockwise

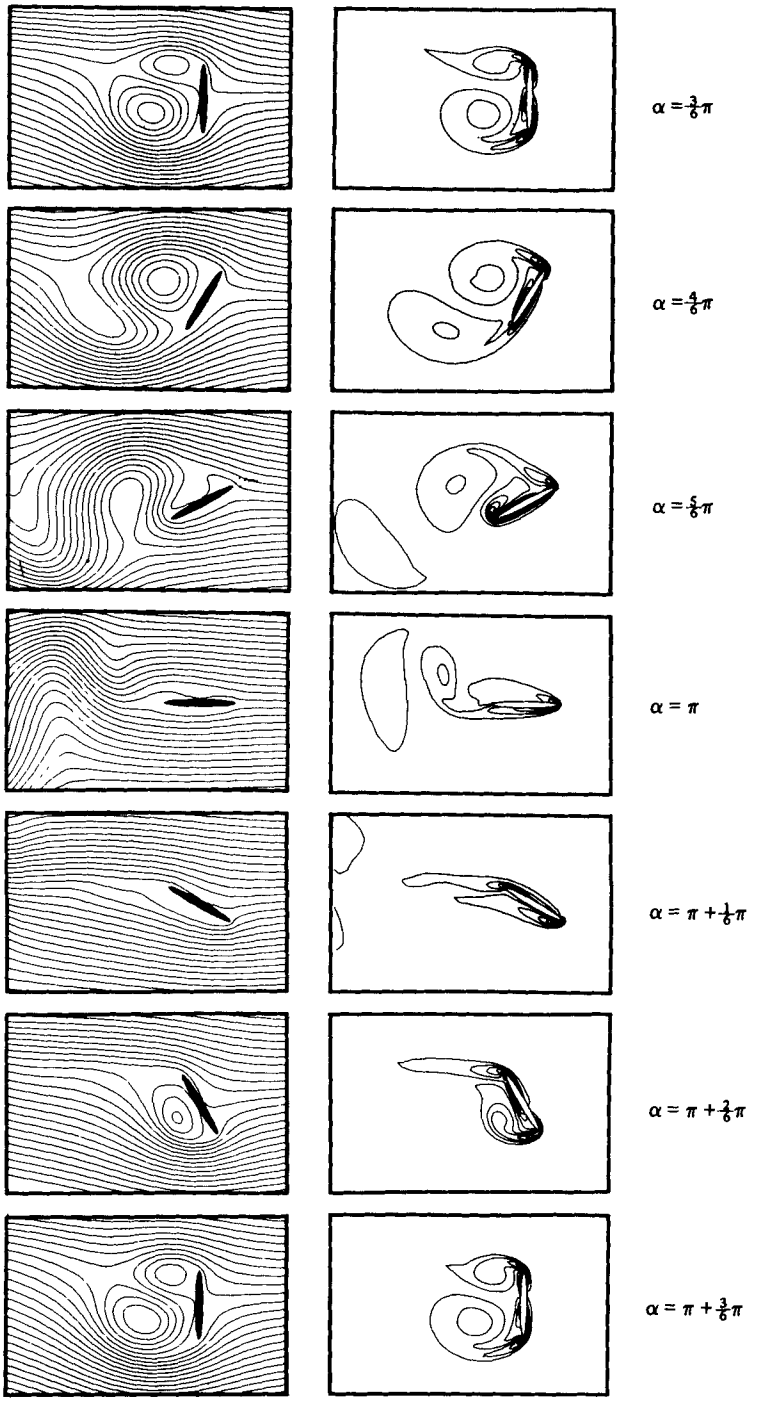

FIGURE 10. Sequence of streamlines and equi-vorticity lines for $S = 0{\cdot}167$, $Re = 200$, $\eta_1 = 0{\cdot}1$, $\alpha_0 = 0°$.

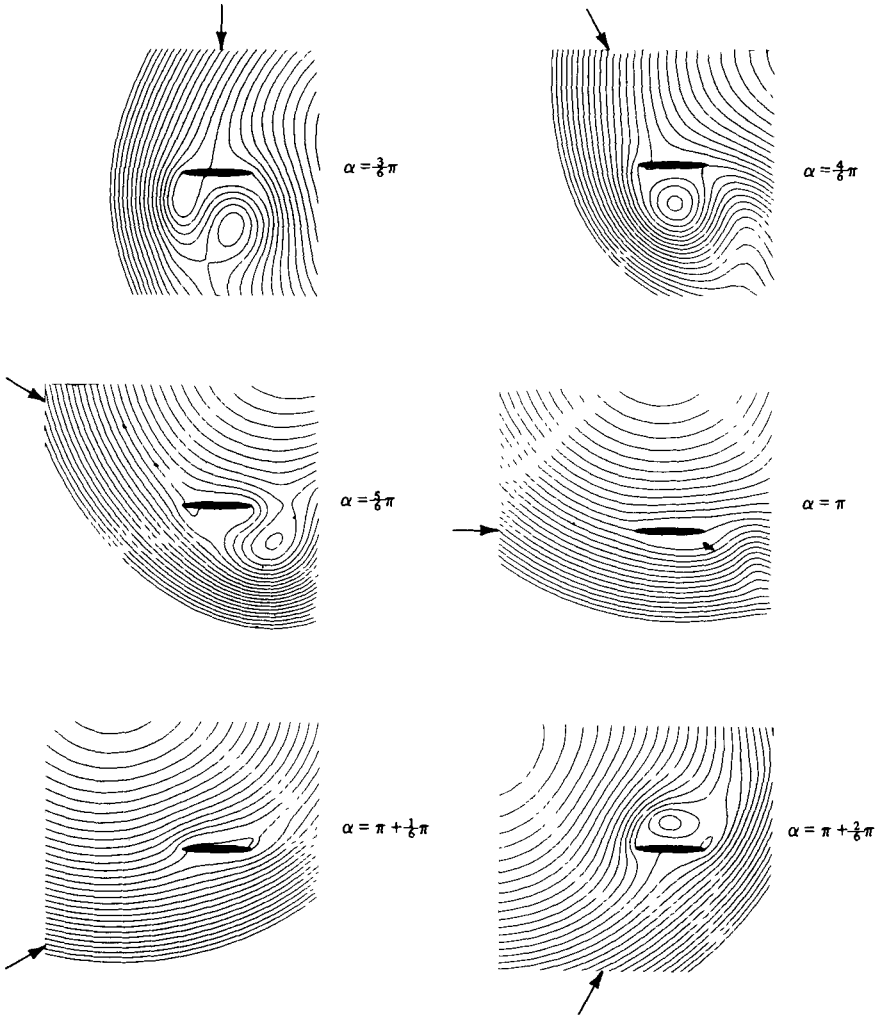

FIGURE 11. Same situation as in figure 10 but streamlines are computed in a frame fixed to the body.

direction is barely visible but becomes more pronounced for $\alpha = 4\pi$. In figure 10, $\alpha = \frac{8}{3}\pi$, the tongue in the clockwise direction can clearly be seen.) For $S \geqslant 1$, $Re = 200$ the relative rate of rotation is so fast that vortices shed from the edges of the plate do not have time to leave the vicinity of the plate and are trapped by the approach of the other edge and then shed. According to figure 5, under these conditions the plate requires an outside driving torque to rotate. For smaller S, probably $S < 0{\cdot}167$, the rotation relative to translation is so slow that the frequency of vortex shedding is larger than the rate of rotation. From figure 5 it appears that $\bar{C}_M$ becomes positive for $S < 0{\cdot}167$ (see also figure 1). In the region $0{\cdot}167 \leqslant S \leqslant 0{\cdot}5$, $Re = 200$ synchronization occurs. The frequency of vortex shedding adjusts to the rate of rotation. This phenomenon has been called 'lock-in' in the study of oscillating bodies in a parallel flow (Griffin & Ramberg 1974). In this range of S autorotation occurs. Hence,

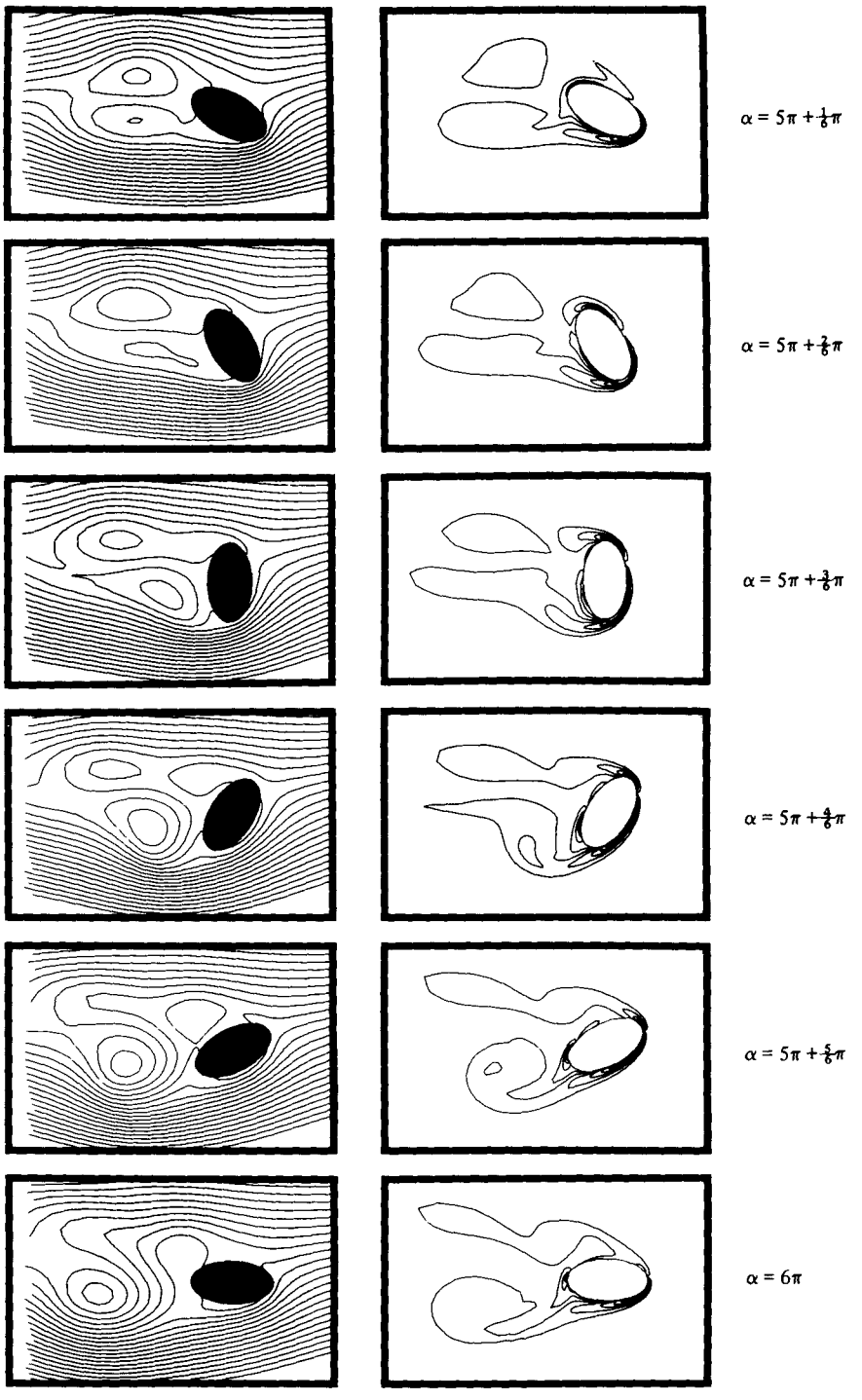

FIGURE 12. Sequence of streamlines and equi-vorticity lines for $S = 0{\cdot}5$, $Re_d = 200$, $\eta_1 = 0{\cdot}6$, $\alpha_0 = 0°$.

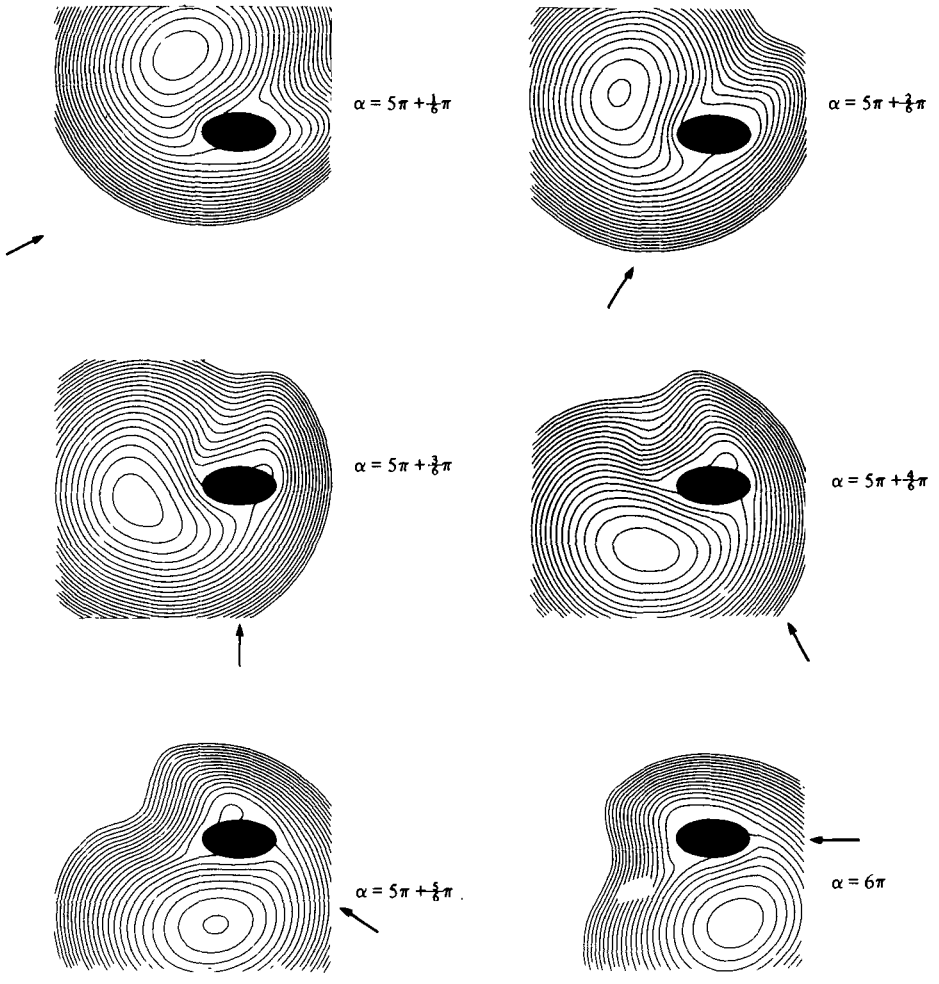

FIGURE 13. Same situation as in figure 12 but streamlines are computed in a frame fixed to the body.

synchronization is a necessary, but not sufficient, condition for autorotation, as the case of a wobbling plate demonstrates.

What mechanism provides excess torque in the shaded region of figure 5 and damping in other regions? This question will be addressed by discussing the supporting and retarding period separately.

(*a*) *Supporting period*

In viscous fluid flows the torque is much smaller than in potential flows during both the supporting and retarding periods because the centre of pressure in the rear of the body is generally closer to the body centre than it is in potential flow (stagnation points in figures 7 and 9). Viscosity modifies the flow characteristics in the supporting period in the following way: behind the leading (retreating) edge a vorticity tongue is visible which owes its existence to the boundary layer in front of the edge. The faster the rotation, the more closely the tongue clings to the rear of the edge since the vorticity

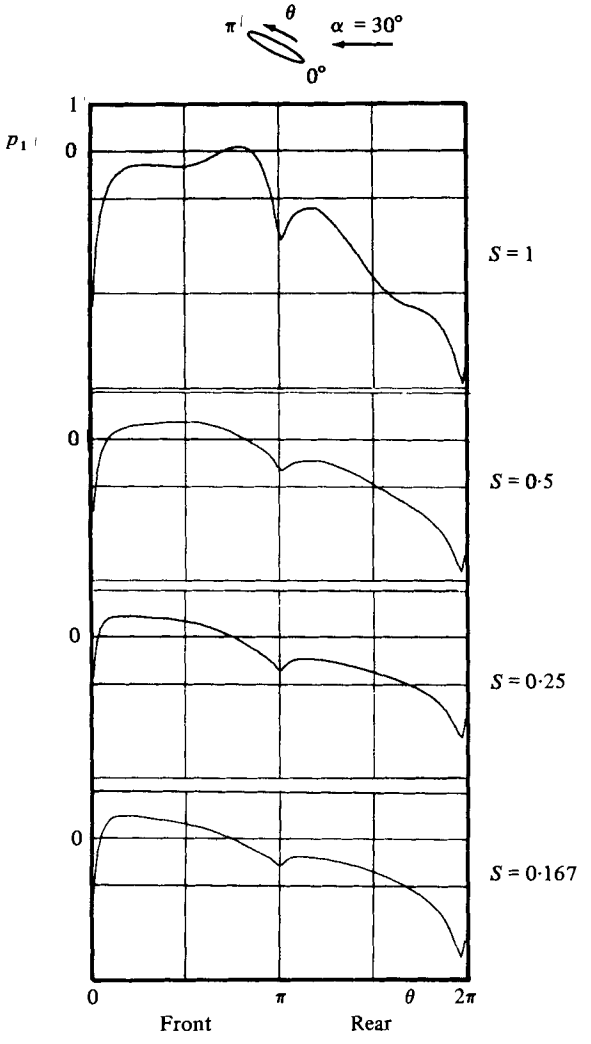

FIGURE 14. Surface pressure p_1 versus θ for various S at $Re = 200$, $\eta_1 = 0{\cdot}1$, and $\alpha = 30°$.

has not enough time to be convected downstream (lower edge in figure 6, $\alpha = 3\pi + \frac{2}{6}\pi$; figure 8, $\alpha = 2\pi + \frac{2}{6}\pi$; figure 10, $\alpha = \pi + \frac{2}{6}\pi$). This clinging causes a higher suction effect behind the edge.

This clinging may also be explained in the following way. With faster rotation vortex separation (stall), which is defined by the first occurrence of a vorticity extremum inside the fluid, is delayed. This delay is caused by the acceleration of fluid with growing α, resulting in a reduction of the adverse pressure gradient (A. M. O. Smith 1953). For instance, for $S = 0{\cdot}5$, $Re = 200$, the vortex at the leading edge separates between 60° and 75° (figure 8, $\alpha = 2\pi + \frac{2}{6}\pi$. Hence, higher S favours autorotation because of the lower surface pressure p_1 behind the edge (figure 14).

Around the advancing edge differences in the surface pressure due to the various shapes of the vorticity tongue are negligible except for $S \geqslant 1$. Here, the vortices from the preceding cycle (upper edge in figure 6, $\alpha = 3\pi + \frac{2}{6}\pi$) cause a lower pressure region

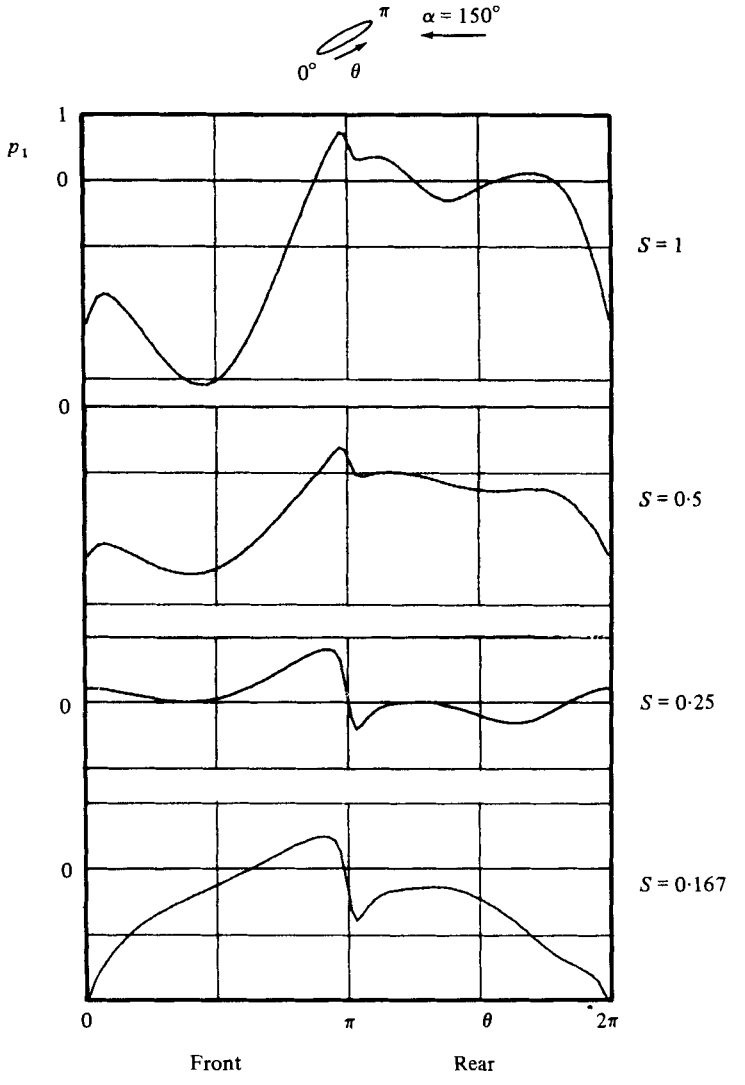

FIGURE 15. Surface pressure p_1 versus θ for various S at $Re = 200$, $\eta_1 = 0{\cdot}1$, and $\alpha = 150°$.

with an adverse effect on autorotation (figure 14). To a certain extent this effect counteracts for $S = 1$ the advantage of the delay of vortex shedding at the other edge. As a result, $\bar{C}_{MS}$ in figure 5 decreases only slightly with larger S. This indicates (and will be later elaborated on) that a local event like delayed vortex shedding behind the retreating edge by itself is not sufficient to explain autorotation. Rather, the interplay of all parts of the flow field must be considered.

(*b*) *Retarding period*

According to figure 4 the major differences among the various S-cases occur in the retarding period. It is here that viscous effects determine the balance between $\bar{C}_{MR}$ and $|\bar{C}_{MS}|$, and thus the occurrence of autorotation.

When the supporting period changes to the retarding period at $\alpha \approx \frac{1}{2}\pi$, the delay of vortex separation around the retreating edge plays an important role in the distribution of the surface pressure (figure 15). For small and large S vortex separation is either too early or too late in the critical α range between 120° and 150°. For large S a new, counter-clockwise vortex develops, whereas for small S a new, clockwise vortex appears (vorticity tongue at the lower edge in figure 6, $\alpha = 3\pi + \frac{5}{6}\pi$, and figure 10, $\alpha = \frac{5}{6}\pi$). In both cases the very low surface pressure in front of the retreating edge counteracts autorotation. (In connexion with figure 15, it may be mentioned that for all cases the local torque contribution $-p_1 \sin 2\theta/\cosh^2 \eta_1$ was computed, but is not presented here.) The existence of another stagnation point for $S = 1$ in figure 15 near $\theta = 15°$ is due to the presence of the newly generated vorticity tongue while the other vortex has not yet moved out of the way (figure 6, $\alpha = 3\pi + \frac{5}{6}\pi$, lower edge).

In the intermediate S-range, however, vortex separation occurs at just the right moment. The flow and pressure distribution for $120° \leqslant \alpha \leqslant 150°$ are then similar to those behind a flat plate parallel to the stream (indicated in figure 8, $\alpha = 2\pi + \frac{5}{6}\pi$ for $S = 0{\cdot}5$, figure 15, $S = 0{\cdot}25$). This optimum situation for autorotation occurs at $S = 0{\cdot}25$. The diminished variation in the surface pressure reduces the adverse effect of the retarding period.

This peculiar situation does not occur in the supporting period, when there is always an asymmetric flow around the edges (see § 3*a*). In the supporting period asymmetry favours autorotation because of the suction effect. The knowledge that $|\bar{C}_{MS}| - \bar{C}_{MR} > 0$ can be obtained only by actually computing the moment coefficients. The difference between $|C_{MS}|$ and C_{MR} at a certain α may be called 'torque hysteresis'.

How delicate the balance between $\bar{C}_{MS}$ and $\bar{C}_{MR}$ is, and how unpredictable the outcome is without computation, is demonstrated by the effect of the leading edge on autorotation in the retarding period. Here early separation of a vortex favours autorotation. In the initial phase, however, with $\alpha_0 = 90°$ (Lugt & Ohring 1977) the vortex behind the leading edge is close to the plate and much stronger at later times. During this period the plate does not autorotate.

As in the supporting period, the above situation shows that the delay of vortex shedding at the retreating edge by itself is insufficient to describe autorotation. The effect of premature vortex shedding at the other edge must be considered too. Therefore the term 'torque hysteresis' is preferred over 'lift hysteresis', which only refers to the delayed vortex separation behind the leading edge of a wing.

Another example of the delicate balance between $\bar{C}_{MR}$ and $\bar{C}_{MS}$ is the influence of the sharpness of the edges on autorotation (Riabouchinsky 1935). It is well known that plates with sharp edges autorotate better (that is, faster) than those with blunt edges, and that blunt bodies do not necessarily autorotate. In order to study this effect, flows around a thick elliptic cylinder were investigated.

In the limit $\eta_1 \to \infty$ the elliptic cylinder becomes a circular one. The distinction between retarding and supporting periods disappears, and the torque is always positive, at least for the Oseen-type flow (Lugt & Ohring 1977) and the special cases studied by Thoman & Szewczyk (1966). The fat ellipse $\eta_1 = 0{\cdot}6$ has been selected as a typical example of conditions between the extremes $\eta_1 = 0$ and $\eta_1 = \infty$. From simple geometrical considerations one expects that tip effects are no longer pronounced and that the larger surface area (when d is kept constant) has an adverse effect on

autorotation. Dynamically speaking, one expects for $\eta_1 = 0{\cdot}6$ less concentration of vorticity around the blunt tips.

Calculations show that $\bar{C}_M = 0{\cdot}178$ for $S = 0{\cdot}5$, $Re_d = 200$, and $\eta_1 = 0{\cdot}6$. Therefore, this body does not autorotate. However, with an amplitude of about 0·9 for C_M the difference between $\bar{C}_{MR} = 0{\cdot}435$ and $|\bar{C}_{MS}| = 0{\cdot}257$ is not as dramatic as one might expect. This means that the curvature effects are rather subtle, and this is confirmed by calculations. It appears that the vortex behind the retreating tip is weaker for $\eta_1 = 0{\cdot}6$ than for $\eta_1 = 0{\cdot}1$ (figure 12, $\alpha = 5\pi + \frac{2}{6}\pi$, lower edge), and that this is the major cause for the small value of $|\bar{C}_{MS}|$. The fact that the thick ellipse does not autorotate for $S = 0{\cdot}5$, $Re_d = 200$, does not mean, however, that it cannot autorotate at all. It is still possible that it could autorotate for smaller S and $\Omega \neq$ const. The autorotation of blunt bodies like hailstones suggests this (Kry & List 1974). Recently, Taneda (1977) published photographs of streamlines and streaklines of elliptic cylinders with $\eta_1 = 0{\cdot}55$ rotating with constant Ω in a parallel flow. These experiments were carried out for $Re_d = 41$, $S = 0{\cdot}17$; $Re_d = 129$, $S = 0{\cdot}5$; and $Re_d = 140$, $S = 0{\cdot}05$. It appears that synchronization occurs even for the small spin parameter 0·05, in contrast to the results obtained for $\eta_1 = 0{\cdot}1$, where synchronization is restricted to $0{\cdot}25 \leqslant S \leqslant 0{\cdot}5$ for $Re = 200$.

The case $S = 0{\cdot}5$, $Re = 400$, $\eta_1 = 0{\cdot}1$ has been chosen to study the effect of Reynolds numbers on autorotation. There are no essential differences between $Re = 200$ and 400, neither with respect to the force and moment coefficients (figure 3) nor with respect to flow patterns (figure 8; for $Re = 200$ see Lugt & Ohring 1977). In fact, a comparison of C_D and C_L curves for $Re = 200$ with the corresponding experimental data for $Re = 90\,000$ from E. H. Smith (1971) reveals a surprisingly good agreement (figure 16). Also, the flow patterns are strikingly similar. The spin coefficient, however, is larger in the experiments by E. H. Smith and other investigators for large Reynolds numbers: $S \approx 0{\cdot}8$ to 1·0 (Iversen 1979).

The insensitivity of unsteady large-scale vortex structures in laminar flows, which is demonstrated here for autorotation, has recently been observed for accelerated wings under high angle of attack (Lugt & Haussling 1978). The small-scale structure appears to be of only secondary importance on the gross flow patterns and on the force and lift coefficients.

4. Conclusions

Autorotation of plates normal to a parallel flow occurs under the following conditions.

(*a*) A necessary but not sufficient condition for autorotation is the synchronization of vortex shedding and rate of rotation. A lock-in effect is observed over a certain S-range, in which the frequency of vortex shedding adjusts to the rate of rotation. This S-range roughly coincides with the shaded area in figure 5.

(*b*) The vortex behaviour at the retreating edge of the plate is crucial for autorotation. In the supporting period a strong, attached vortex behind the retreating edge helps autorotation. In the retarding period the timing of its shedding is important. Premature shedding (for small S) or delayed shedding (for large S) results in an asymmetric flow past the retreating edge ($120° < \alpha < 150°$) with low pressure at the edge which has an adverse effect on autorotation. Under condition (*a*), however, the flow past the retreating edge is quite symmetric, and the pressure on both sides of

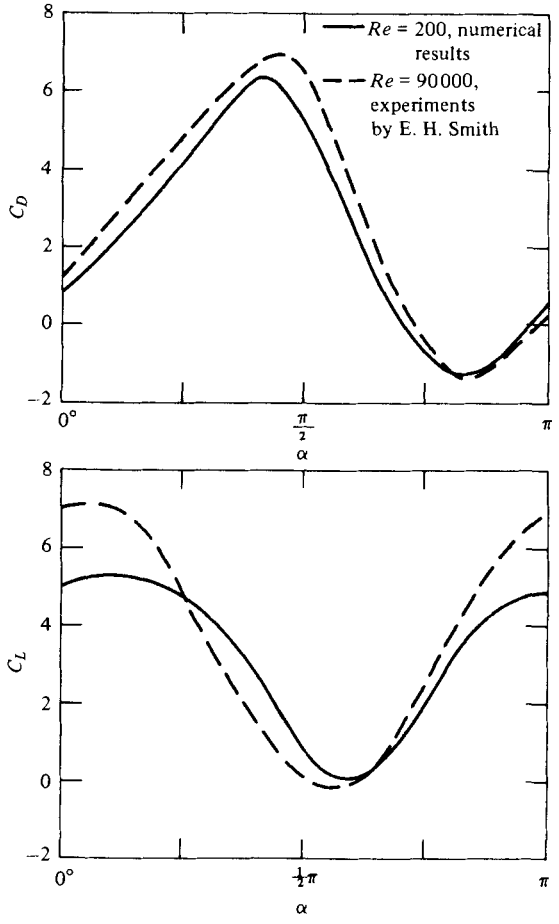

FIGURE 16. C_D and C_L for one cycle. Comparison of numerical results for $Re = 200$, $\eta_1 = 0{\cdot}1$ with experimental data for $Re = 90000$, $\eta_1 = 0{\cdot}15$ from E. H. Smith (1971).

the plate is balanced. This situation reduces the adverse torque in the retarding period.

(*c*) The attached vortex behind the retreating edge in the supporting period favours autorotation according to (*b*). Rounded edges weaken this vortex. Thus, a sharp edge is most favourable for autorotation. The fat elliptical cylinder $\eta_1 = 0{\cdot}6$ does not autorotate for $S = 0{\cdot}5$, $Re_d = 200$, and $\Omega = \text{const}$.

(*d*) The parameter I^*S^2 must be sufficiently large so that condition (6) is satisfied.

(*e*) Autorotation requires the fulfilment of all conditions (*a*) through (*d*). The actual occurrence and the exact rate of autorotation are determined by a delicate and intricate interplay of factors (*a*) through (*d*). For $Re_d = 200$, $\eta_1 = 0{\cdot}1$, and $\Omega = \text{const.}$, stable autorotation occurs at $S \approx 0{\cdot}45$.

Reynolds-number effects on the force and moment coefficients as well as on large-scale vortex structures are probably small over the range $200 \leqslant Re_d \leqslant 90000$. According to E. H. Smith (1971) (whose data have been corrected by Iversen 1979) and other investigators, the spin parameter is about 0·8 to 1·0 for Reynolds numbers much larger than 200.

REFERENCES

BAIRSTOW, L. 1939 *Applied Aerodynamics*, 2nd edn, cha. V, p. 212. London: Longman.

GRIFFIN, O. M. & RAMBERG, S. E. 1974 The vortex-street wakes of vibrating cylinders. *J. Fluid Mech.* **66**, 553.

IVERSEN, J. D. 1979 Autorotating flat-plate wings: the effect of the moment of inertia, geometry and Reynolds number. *J. Fluid Mech.* **92**, 327.

KRY, P. R. & LIST, R. 1974 Angular motions of freely falling spheroidal hailstone models. *Phys. Fluids* **17**, 1093.

LAMB, H. 1945 *Hydrodynamics*, 6th edn. Dover.

LUGT, H. J. 1978 Autorotation of plates. *David W. Taylor Naval Ship R & D Center Rep.* no. 78/058.

LUGT, H. J. & HAUSSLING, H. J. 1974 Laminar flow past an abruptly accelerated elliptic cylinder at 45° incidence. *J. Fluid Mech.* **65**, 711.

LUGT, H. J. & HAUSSLING, H. J. 1978 The acceleration of thin cylindrical bodies in a viscous fluid. *J. Appl. Mech.* **45**, 1.

LUGT, H. J. & OHRING, S. 1977 Rotating elliptic cylinders in a viscous fluid at rest or in a parallel stream. *J. Fluid Mech.* **79**, 127.

MAXWELL, J. C. 1890 On a particular case of the descent of a heavy body in a resisting medium. *Scientific Papers*, p. 115. Cambridge University Press.

RIABOUCHINSKY, D. P. 1935 Thirty years of theoretical and experimental research in fluid mechanics. *J. Roy. Aero. Soc.* **39**, 282.

SMITH, A. M. O. 1953 On the motion of a tumbling body. *J. Aero. Sci.* **20**, 73.

SMITH, E. H. 1971 Autorotating wings: an experimental investigation. *J. Fluid Mech.* **50**, 513.

TANEDA, S. 1977 Visual study of unsteady separated flows around bodies. *Prog. Aero. Sci.* **17**, 287.

THOMAN, D. C. & SZEWCZYK, A. A. 1966 Numerical solutions of time dependent two dimensional flow of a viscous, incompressible fluid over stationary and rotating cylinders. *Univ. Notre Dame, Dept. Mech. Engng Tech. Rep.* no. 66–14.